orientation and spatial frequency tuning, at each recording site for each animal. The temporal impulse functions were derived by generating a histogram of the neural responses to briefly presented flashes at random positions within the receptive field. Identical results were obtained with filters defined by parameters that were based on data obtained at each of the three age groups. The shapes of the correlational functions were relatively insensitive to the particular parameter values of the spatial and temporal filters.

Oscillation analysis

Oscillation frequency was computed separately at each recording site. First, discriminated spikes were placed into 2-ms bins. 800-ms windows of binned spikes were extracted every 200 ms, and the autocorrelation of the windowed spikes was computed, followed by the fast Fourier transform (FFT). The frequency with the maximum amplitude was determined, and a histogram of these frequencies was constructed.

Received 3 May; accepted 30 July 2004; doi:10.1038/nature02907.

1. Henry, G. H., Bishop, P. O., Tupper, R. M. & Dreher, B. Orientation specificity and response variability of cells in striate cortex. *Vision Res.* **13,** 1771–1779 (1973).
2. Schiller, P. H., Finlay, B. L. & Volman, S. F. Short-term response variability of monkey striate neurons. *Brain Res.* **105,** 347–349 (1976).
3. Vogels, R., Spileers, W. & Orban, G. A. The response variability of striate cortical neurons in the behaving monkey. *Exp. Brain Res.* **77,** 432–436 (1989).
4. Azouz, R. & Gray, C. M. Cellular mechanisms contributing to response variability of cortical neurons *in vivo*. *J. Neurosci.* **19,** 2209–2223 (1999).
5. Zohary, E., Shadlen, M. N. & Newsome, W. T. Correlated neuronal discharge rate and its implications for psychophysical performance. *Nature* **370,** 140–143 (1994).
6. Shadlen, M. N. & Newsome, W. T. The variable discharge of cortical neurons: Implications for connectivity, computation, and information coding. *J. Neurosci.* **18,** 3870–3896 (1998).
7. Pouget, A., Dayan, P. & Zemel, R. Inference and computation with population codes. *Annu. Rev. Neurosci.* **26,** 381–410 (2004).
8. Meister, M., Wong, R. O. L., Baylor, D. A. & Shatz, C. J. Synchronous bursts of action potentials in ganglion cells of the developing mammalian retina. *Science* **252,** 939–943 (1991).
9. Arieli, A., Shoham, D., Hildesheim, R. & Grinvald, A. Coherent spatiotemporal patterns of ongoing activity revealed by real-time optical imaging coupled with single-unit recording in the cat visual cortex. *J. Neurophysiol.* **73,** 2072–2093 (1995).
10. Weliky, M. & Katz, L. C. Correlational structure of spontaneous neuronal activity in the developing lateral geniculate nucleus *in vivo*. *Science* **285,** 599–604 (1999).
11. Tsodyks, M., Kenet, T., Grinvald, A. & Arieli, A. Linking spontaneous activity of single cortical neurons and the underlying functional architecture. *Science* **286,** 1943–1946 (1999).
12. Chiu, C. & Weliky, M. Spontaneous activity in developing ferret visual cortex *in vivo*. *J. Neurosci.* **21,** 8906–8914 (2001).
13. Kenet, T., Bibitchkov, D., Tsodyks, M., Grinvald, A. & Arieli, A. Spontaneously emerging cortical representations of visual attributes. *Nature* **425,** 954–956 (2003).
14. Gao, W., Newman, D. E., Wormington, A. B. & Pallas, S. Development of inhibitory circuitry in visual and auditory cortex of postnatal ferrets: Immunocytochemical localization of GABAergic neurons. *J. Comp. Neurol.* **409,** 261–273 (1999).
15. Anderson, J., Lampl, I., Reichova, I., Carandini, M. & Ferster, D. Stimulus dependence of two-state fluctuations of membrane potential in cat visual cortex. *Nature Neurosci.* **3,** 617–621 (2000).
16. Cossart, R., Aronov, D. & Yuste, R. Attractor dynamics of network UP states in the neocortex. *Nature* **423,** 283–288 (2003).
17. Shu, Y. S., Hasenstaub, A., Badoual, M., Bal, T. & McCormick, D. A. Barrages of synaptic activity control the gain and sensitivity of cortical neurons. *J. Neurosci.* **23,** 10388–10401 (2003).
18. Gallant, J. L., Connor, C. E. & Van Essen, D. C. Neural activity in areas V1, V2 and V4 during free viewing of natural scenes compared to controlled viewing. *Neuroreport* **9,** 1673–1678 (1998).
19. Vinje, W. E. & Gallant, J. L. Sparse coding and decorrelation in primary visual cortex during natural vision. *Science* **287,** 1273–1276 (2000).
20. Gawne, T. J. & Richmond, B. J. How independent are the messages carried by adjacent inferior temporal cortical neurons? *J. Neurosci.* **13,** 2758–2771 (1993).
21. Pola, G., Thiele, A., Hoffmann, K. P. & Panzeri, S. An exact method to quantify the information transmitted by different mechanisms of correlational coding. *Network Comput. Neural Syst.* **14,** 35–60 (2003).
22. Nirenberg, S. & Latham, P. E. Decoding neuronal spike trains: How important are correlations? *Proc Natl Acad. Sci. USA* **100,** 1045–1050 (2003).
23. Kara, P., Reinagel, P. & Reid, R. C. Low response variability in simultaneously recorded retinal, thalamic, and cortical neurons. *Neuron* **27,** 635–646 (2000).
24. Hirsch, J. A. *et al.* Synaptic physiology of the flow of information in the cat's visual cortex *in vivo*. *J. Physiol. (Lond.)* **540,** 335–350 (2002).
25. Attwell, D. & Laughlin, S. B. An energy budget for signaling in the grey matter of the brain. *J. Cereb. Blood Flow Metab.* **21,** 1133–1145 (2001).
26. Lennie, P. The cost of cortical computation. *Curr. Biol.* **13,** 493–497 (2003).
27. Weliky, M., Fiser, J., Hunt, R. H. & Wagner, D. N. Coding of natural scenes in primary visual cortex. *Neuron* **37,** 703–718 (2003).

Supplementary Information accompanies the paper on **www.nature.com/nature**.

Acknowledgements This work was supported by NIH (NEI) and the McKnight Foundation. We thank David Wagner for technical assistance. We also thank R. Aslin, D. Knill, D. Lee and K. Nordeen for comments. We also thank E. Romanski for supplying the ISCAN equipment.

Competing interests statement The authors declare that they have no competing financial interests.

Correspondence and requests for materials should be addressed to M.W. (weliky@cvs.rochester.edu).

A transmembrane protein required for acetylcholine receptor clustering in *Caenorhabditis elegans*

Christelle Gally[1], Stefan Eimer[1], Janet E. Richmond[2] & Jean-Louis Bessereau[1]

[1]*INSERM U.497, École Normale Supérieure, 46 rue d'Ulm, 75005 Paris, France*
[2]*University of Illinois at Chicago, Chicago, Illinois 60607, USA*

Clustering neurotransmitter receptors at the synapse is crucial for efficient neurotransmission. Here we identify a *Caenorhabditis elegans* locus, *lev-10*, required for postsynaptic aggregation of ionotropic acetylcholine receptors (AChRs). *lev-10* mutants were identified on the basis of weak resistance to the anthelminthic drug levamisole, a nematode-specific cholinergic agonist that activates AChRs present at neuromuscular junctions (NMJs) resulting in muscle hypercontraction and death at high concentrations[1–3]. In *lev-10* mutants, the density of levamisole-sensitive AChRs at NMJs is markedly reduced, yet the number of functional AChRs present at the muscle cell surface remains unchanged. LEV-10 is a transmembrane protein localized to cholinergic NMJs and required in body-wall muscles for AChR clustering. We also show that the LEV-10 extracellular region, containing five predicted CUB domains and one LDLa domain, is sufficient to rescue AChR aggregation in *lev-10* mutants. This suggests a mechanism for AChR clustering that relies on extracellular protein–protein interactions. Such a mechanism is likely to be evolutionarily conserved because CUB/LDL transmembrane proteins similar to LEV-10, but lacking any assigned function, are expressed in the mammalian nervous system and might be used to cluster ionotropic receptors in vertebrates.

Genetic screens for *C. elegans* mutants that exhibit strong resistance to levamisole have identified four genes encoding AChR subunits and two genes that are required for the biosynthesis of levamisole-sensitive AChRs[1–3]. However, no genes required for AChR clustering were cloned despite the large size of these screens. We hypothesized that impairing the function of such genes would generate subtle phenotypes for two reasons. First, unclustered levamisole-sensitive AChRs might remain functional if properly inserted into the plasma membrane, thus conferring levamisole-sensitivity. Second, there is an additional class of AChRs present at *C. elegans* NMJs that are activated by acetylcholine and nicotine but are insensitive to levamisole[4]. These receptors, of as yet unknown composition, might compensate for a decrease in levamisole-sensitive AChRs at the synapse.

We therefore performed a screen to isolate mutants that exhibited only weak resistance to levamisole. To facilitate the identification of mutated genes we used an insertional mutagenesis based on germline mobilization of the *Drosophila* transposon *Mos1* (ref. 5). We isolated a mutant allele, *kr26*, that resulted from a *Mos1* insertion whose interpolated genetic position was in the vicinity of the *lev-10* locus. A single mutant allele of *lev-10*, *x17*, was isolated previously in a levamisole-resistance screen but was not characterized at the molecular level[1]. Using a genetic complementation test, we showed that *x17* and *kr26* are two alleles of the same gene, *lev-10*. Both *lev-10* mutants displayed a slight resistance to levamisole, when assayed by dose–response (Fig. 1a), but after 1 h of exposure to 1 mM levamisole, 100% of the *lev-10* mutants became paralysed. Although, in contrast to wild-type animals, *lev-10* mutants were able to survive while remaining hypercontracted at this elevated drug concentration. In addition, both *lev-10* mutants displayed marginal locomotory defects on plates. When movement was analysed in liquid medium, a subtle but significant movement impairment was

detected (Fig. 1b). These phenotypes suggested that mutating *lev-10* only partly impairs the function of levamisole-sensitive AChRs.

To analyse the expression of these receptors, we raised antibodies against UNC-29, a non-α-subunit of the levamisole-sensitive AChR in muscle[6]. In wild-type animals, UNC-29 was clustered along the ventral and dorsal cords and in the nerve ring where head muscles are innervated (Fig. 2a, c). In *lev-10* mutants, no detectable UNC-29 staining was observed along the ventral and dorsal nerve cords, and only weak staining remained in the nerve ring (Fig. 2b, d). To test whether the loss of UNC-29 clusters in *lev-10* mutants was due to the absence of cholinergic innervation, we immunostained cholinergic varicosities with an antibody against UNC-17, the vesicular acetylcholine transporter in *C. elegans*[7]. Staining patterns were similar in wild-type (Fig. 2e) and *lev-10* mutant animals (Fig. 2f). In addition to cholinergic innervation, body-wall muscles are also innervated by GABAergic motoneurons. To determine whether *lev-10* was globally required for the formation of receptor aggregates or was specifically acting at cholinergic neuromuscular synapses, we immunostained the muscle $GABA_A$ receptor UNC-49 (refs 8, 9). In both the wild type and *lev-10* mutants, GABA receptors were clustered along the nerve cords (Fig. 2g, h). The inability to detect AChRs by immunostaining could result from decreased receptor expression in *lev-10* mutants. Alternatively, a diffuse distribution of a wild-type number of receptors could be below our detection threshold. AChR expression was therefore assessed by western blot analysis of fractionated worm extracts (Fig. 2i). In *lev-10(kr26)* and *lev-10(x17)* extracts, the UNC-29 concentrations were similar to that in the wild type (90 ± 12% ($n = 4$) and 123 ± 17% ($n = 4$), respectively), suggesting that AChR expression is not reduced in *lev-10* mutants.

To test whether the UNC-29 protein detected in *lev-10* mutants was assembled into functional receptors present at the muscle cell surface, we used electrophysiology[4]. Pressure-ejection of levamisole onto voltage-clamped body-wall muscles elicited similar currents in the wild type and in *lev-10* mutants (Fig. 3a, b), whereas in a *unc-29 lev-10* double mutant no levamisole current was detected (data not shown). These data indicate that the overall expression level of functional levamisole-sensitive AChRs in *lev-10* mutants is comparable to that in the wild type. To analyse the synaptic population of levamisole-sensitive AChRs, we stimulated motoneurons in the ventral cord and recorded evoked currents in individual muscle cells. To eliminate currents due to activation of the GABA receptor UNC-49, we performed our analysis in an *unc-49(e407)* null mutant background. Furthermore, we used the nicotinic antagonist dihydro-β-erythroidine (DHβE) to block levamisole-insensitive AChRs present at NMJs[4]. In *lev-10;unc-49* double mutants, the size of the evoked response in the presence of DHβE was decreased by 77% compared with that of *unc-49* (Fig. 3c, d). The remaining evoked current was due to the activation of levamisole-sensitive AChRs, because *unc-29;unc-49* double mutants, which no longer

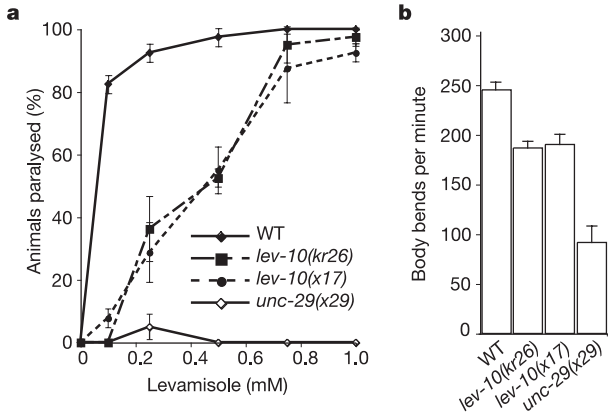

Figure 1 Phenotypic characterization of *lev-10* mutants. **a**, The levamisole dose–response curve indicates that *lev-10* mutants are only weakly resistant to levamisole when compared with *unc-29(x29)* mutants, which lack levamisole-sensitive AChRs. Error bars represent s.e.m. ($n = 4$ independent experiments). WT, wild type. **b**, *lev-10* mutants exhibit weak locomotory defects compared with the wild type in a thrashing assay (ANOVA test; $p < 0.01$) but are not as impaired as *unc-29(x29)* mutants ($p < 0.01$). Error bars represent s.e.m. ($n = 6$).

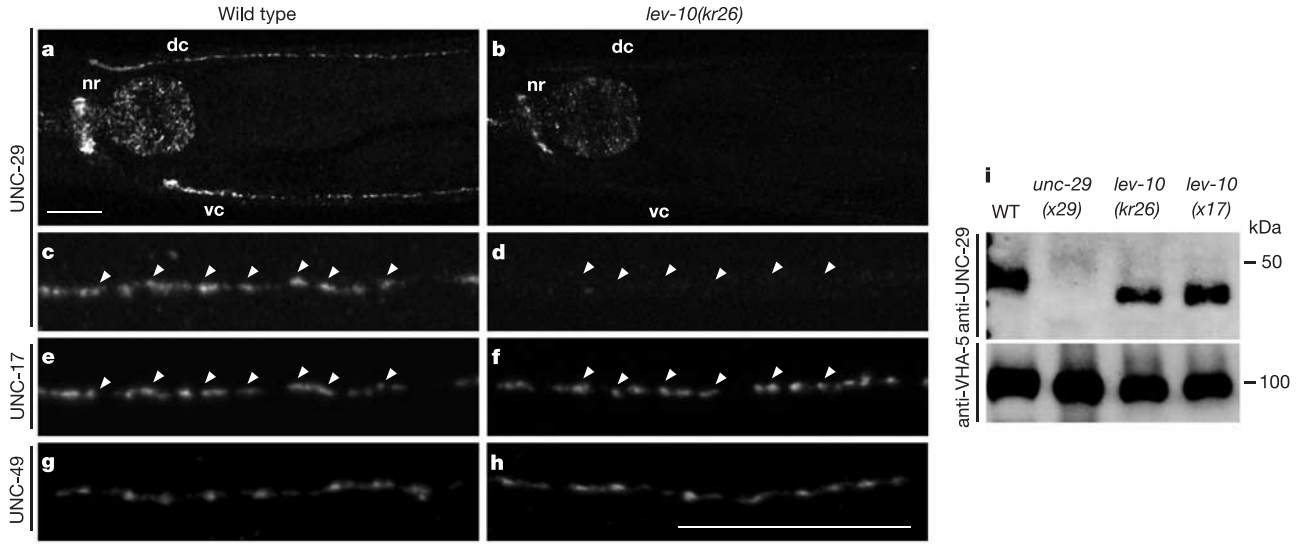

Figure 2 Mutation of *lev-10* results in the specific loss of levamisole-sensitive AChR clusters at neuromuscular junctions. **a**–**d**, UNC-29 localization detected by immunofluorescence with anti-UNC-29 antibodies. **a**, Shown are the nerve ring (nr) and the dorsal (dc) and ventral (vc) nerve cords in wild-type animals. **c**, Individual UNC-29 puncta at high magnification in the dorsal cord from the wild type. **b**, **d**, UNC-29 staining in *lev-10(kr26)* animals at magnifications as in **a** and **c**, respectively. The staining in the pharynx is non-specific (data not shown). **e**, Visualization of cholinergic varicosities by co-immunostaining of the vesicular ACh transporter UNC-17 in wild-type animals shows that UNC-29 clusters are juxtaposed to cholinergic release sites (arrowheads). **f**, UNC-17 staining in *lev-10(kr26)* mutants. **g**, **h**, Immunostaining of the GABA receptor UNC-49 in wild-type animals (**g**) and *lev-10(kr26)* mutants (**h**). Scale bars, 20 μm. **i**, Western blot with anti-UNC-29 and anti-VHA-5 antibodies on membrane fractions of *C. elegans* extracts. The UNC-29 protein has an apparent molecular mass of 47 kDa. VHA-5 detection is used for normalization. WT, wild type.

express levamisole-sensitive AChRs[4], exhibited no evoked response in the presence of DHβE. In addition, the time to peak and decay time of the evoked current were increased in *lev-10;unc-49* compared with those in *unc-49* (6.44 ± 0.41 ms ($n = 7$) versus 4.64 ± 0.18 ms ($n = 7$), $p < 0.0017$, and 16.6 ± 6.9 ms ($n = 6$) versus 8.4 ± 0.43 ms ($n = 7$), $p < 0.0002$, respectively). These kinetic alterations are consistent with a decreased ratio of synaptic versus perisynaptic receptors being activated by synaptic release of acetylcholine in the *lev-10* background. Analysis of evoked response amplitudes in the absence of DHβE in *lev-10;unc-49* and *unc-49* mutants did not reveal any significant difference (3329 ± 221 pA ($n = 6$) versus 2904 ± 291 pA ($n = 7$), respectively), thus suggesting that the expression and localization of the levamisole-insensitive AChRs present at the NMJ were not affected in *lev-10* mutants. In combination with the immunostaining data, these results indicate that *lev-10* is required specifically for the clustering of levamisole-sensitive AChRs at the synapse.

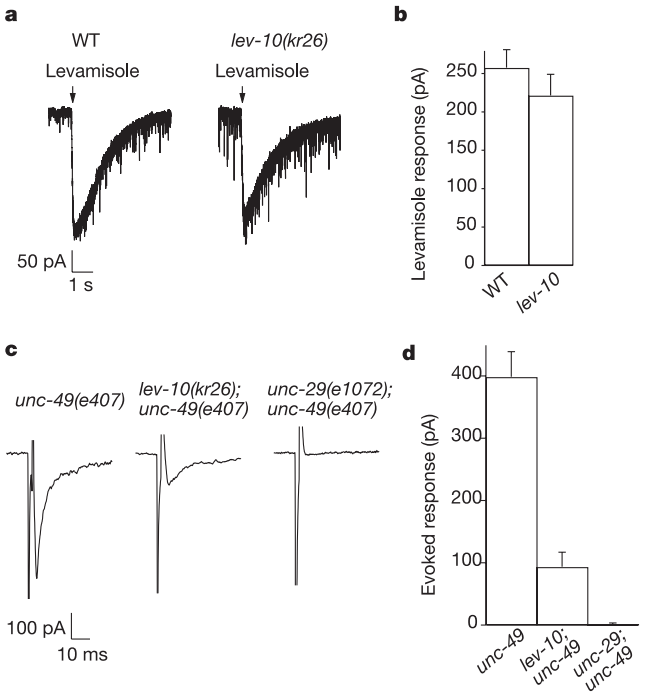

Figure 3 Levamisole-sensitive AChRs are functional but diffusely distributed in *lev-10* body-wall muscle. **a**, Currents recorded from voltage-clamped body wall muscles in response to pressure-ejection of levamisole (300 μM) in wild-type (WT) and *lev-10(kr26)* mutants. **b**, Average amplitude of levamisole-elicited current. **c**, Evoked currents recorded in a body-wall muscle after eliciting neurotransmitter release by ventral nerve cord depolarization. Experiments were performed in an *unc-49(e407)* background to eliminate currents due to GABA receptor activation and in the presence of 5 μM DHβE, which blocks the levamisole-insensitive AChRs. **d**, Average amplitude of evoked response. Error bars in **b** and **d** represent s.e.m.

We cloned *lev-10* using inverse polymerase chain reaction (PCR) to identify the genomic position of the *kr26::Mos1* insertion (Fig. 4a) and confirmed its identity by rescue experiments (Supplementary Table S1). Interestingly, *lev-10* overlaps with *eat-18*, a gene required for the function of AChRs in pharyngeal muscle[10,11]. Mutation of *eat-18* does not confer levamisole resistance. We confirmed that these genes are distinct by genetic complementation (data not shown) and by rescuing *lev-10* mutants with a genomic fragment carrying the *eat-18(ad1110)* nonsense mutation (Supplementary Table S1). *lev-10* is predicted to encode a type I transmembrane protein (Fig. 4b). The extracellular part of the protein contains five predicted CUB domains and one LDLa domain. These domains are present in a wide variety of secreted and membrane-bound proteins and mediate protein–protein interactions (for reviews see refs 12–14). Alternative splicing of *lev-10* generates two transcripts, *lev-10a* and *lev-10b* (Fig. 4b). The *lev-10b* splice variant represents less than 10% of *lev-10* mRNAs (data not shown) and codes for a LEV-10 isoform that differs from LEV-10A in the transmembrane region and contains virtually no intracellular region.

In wild-type animals, LEV-10 is concentrated at cholinergic NMJs (Fig. 5a, c, e). Double labelling experiments with an antibody against the vesicular acetylcholine transporter UNC-17 (ref. 15) demonstrated that 93 ± 3% of LEV-10 puncta were associated with cholinergic varicosities (mean ± SEM, 104 puncta counted in seven worms). However, three-dimensional analysis of confocal image stacks revealed that LEV-10 staining was juxtaposed to, but did not overlap, UNC-17 distribution (Fig. 5f). To determine whether LEV-10 functions postsynaptically, we expressed LEV-10A or LEV-10B under the control of the muscle-specific promoter *myo-3* (ref. 16) in *lev-10(kr26)* animals. Both proteins rescued behavioural defects and UNC-29 synaptic clustering when expressed in muscle (Supplementary Table S1). Genetic mosaic

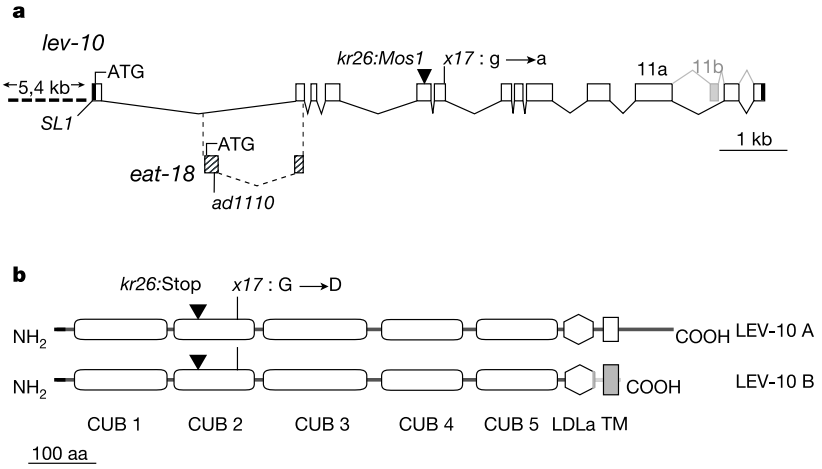

Figure 4 *lev-10* encodes a CUB domain-rich transmembrane protein. **a**, Genomic organization of *lev-10*. Open boxes, coding regions; black boxes, 5′ and 3′ untranslated region; ATG, translational start site; *SL1*, *SL1 trans*-spliced leader. The first intron of *lev-10* contains the first exon of the gene *eat-18* (hatched boxes). The *eat-18* exon is spliced to the second exon of *lev-10* by using a different frame, which ends 16 bp after the splice site. *ad1110*, nonsense mutation in the first exon of *eat-18*. **b**, Predicted structure of the LEV-10 isoforms. Horizontal black line, signal peptide; CUB, complement, urchin epidermal growth factor, and bone morphogenetic protein domain; LDLa, low-density lipoprotein receptor domain class A; TM, transmembrane region; aa, amino acids. Domain predictions were based on SMART (http://smart.embl-heidelberg.de).

analysis (Supplementary Information) confirmed that LEV-10 is required cell autonomously in postsynaptic muscle cells for AChR clustering at NMJs.

Recent results have suggested that proteins involved in neurotransmitter receptor clustering do not accumulate at the synapse in the absence of the receptors[17]. To test this possibility in our system, we analysed the distribution of LEV-10 in animals lacking levamisole-sensitive AChRs. In *unc-29(x29)* and *unc-38(x20)* AChR subunit mutants, no LEV-10 was detected in ventral and dorsal nerve cords by immunofluorescence (Fig. 5b and data not shown) even though presynaptic cholinergic varicosities differentiated normally (Fig. 5d). In parallel, LEV-10 expression level was assessed by western blot analysis (Fig. 5g). LEV-10 was detected as a 120-kDa protein present in the membrane fraction of wild-type worm extracts. This band was absent from *lev-10(kr26)* extracts and was markedly reduced in *lev-10(x17)*. In *unc-29* and *unc-38* extracts, LEV-10 concentrations were decreased only slightly in comparison with those in the wild type (72% ± 11 ($n = 4$) and 81% ± 4 ($n = 5$), respectively), indicating that a lack of levamisole-sensitive AChRs does not alter LEV-10 expression level. Because LEV-10 is expressed but fails to accumulate at synapses in the absence of levamisole-sensitive AChRs, we cannot exclude the possibility that LEV-10 requires AChRs to reach the plasma membrane, although no intracellular staining of LEV-10 is seen by immunofluorescence in *unc-29* and *unc-38* mutants. Alternatively, LEV-10 might interact directly or indirectly with AChRs in a complex that is recruited or stabilized at the synapse.

Because most characterized ionotropic receptor clustering proteins are cytoplasmic, relevant interactions are thought to occur on the cytoplasmic side of the postsynaptic membrane[18,19]. However, complexes formed on the extracellular side of the postsynaptic membrane might also be critical[20–23]. To test this possibility, we fused the extracellular part of LEV-10 to the human CD4 transmembrane domain. Expression of this chimaeric protein in muscle rescued the defects in levamisole sensitivity, locomotion and AChR clustering of *lev-10(kr26)* animals. Furthermore, we overexpressed a green fluorescent protein (GFP)-tagged version of LEV-10 truncated before the transmembrane segment. This protein was secreted from muscle cells into the pseudocoelomic cavity (data not shown) but was still able to rescue *lev-10(kr26)* mutant phenotypes (Supplementary Table S1). The function of LEV-10 in AChR clustering therefore seems to involve only extracellular interactions.

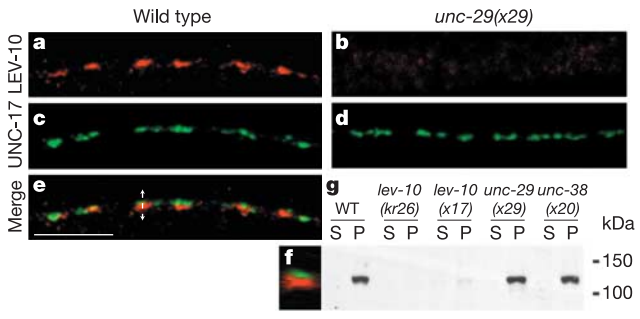

Figure 5 LEV-10 is a synaptic protein that requires levamisole-sensitive AChRs for proper localization but not for expression. **a**, LEV-10A immunostaining in the dorsal cord of a wild-type animal. **c**, UNC-17 immunostaining of the same animal labels cholinergic varicosities. **e**, Merged images. **f**, *Z*-optical projection through the entire stack of confocal images at the level of the dashed arrow in **e**. **b**, **d**, LEV-10A (**b**) and UNC-17 (**d**) immunostaining in the dorsal cord of an *unc-29(x29)* mutant. Scale bar, 10 μm. **g**, Western blot analysis of fractionated *C. elegans* extracts. P, pellet; S, cytosolic supernatant. The LEV-10 transmembrane protein has an apparent molecular mass of about 120 kDa. Mutants of the levamisole-sensitive AChR subunits *unc-29(x29)* and *unc-38(x20)* have LEV-10 concentrations at the membrane comparable to those of the wild type.

LEV-10 is the first example of a CUB/LDL protein involved in the synaptic clustering of AChRs. The presence of multiple predicted protein–protein interaction domains in the extracellular region indicates that LEV-10 might bind multiple partners. Because we have so far been unable to demonstrate direct interactions between LEV-10 and AChRs, LEV-10 might be indirectly involved in the recruitment of signalling molecules that, in turn, cause AChR clustering. However, the interdependence between LEV-10 and AChR for synaptic localization is consistent with a model that would involve a set of interactions between LEV-10, AChRs or AChR-associated proteins, and a synaptic determinant used to nucleate clustering. Along this line, another *C. elegans* CUB-domain-rich transmembrane protein, SOL-1, has recently been shown to physically interact with glutamate receptors and to be required for glutamate-gated currents through an as yet unidentified mechanism[24].

Of 145 CUB-domain-containing mouse proteins present in non-redundant databases, the first two CUB domains of LEV-10 are most similar to those present in NETO2 (ref. 25) (26% identity, 43% similarity). NETO2 and its paralogue NETO1/BTCL1 (refs 25, 26) are predicted type I transmembrane proteins containing two CUB domains and one LDLa domain in their extracellular region. The two *NETO* genes are specifically expressed in retina and brain, but their function is unknown. It is therefore tempting to speculate that LEV-10 and NETO proteins are members of a novel class of membrane-spanning proteins engaged in postsynaptic domain organization by means of extracytoplasmic interactions at the synapse. □

Methods

Cloning of *lev-10*

N2 worms were mutagenized by germline mobilization of the *Drosophila* transposon *Mos1* (ref. 5). Young-adult F2 worms were screened for resistance to 1 mM levamisole 3–5 h after transfer to drug-containing plates. In EN 26 [*lev-10(kr26::Mos1)*], a *Mos1* insertion was localized in a predicted exon of the open reading frame Y105E8A.7a, at position 14,403,250 of chromosome I by using inverse PCR (WormBase, www.wormbase.org).

Rescue experiments were performed with a genomic fragment covering the Y105E8A.7a coding region plus 5 kilobases (kb) upstream of the translational start site and 0.21 kb downstream of the *lev-10a* stop codon. This 15-kb fragment was amplified from N2 or *eat-18(ad1110)*[11] genomic DNA and was injected at 0.85 ng μl^{-1} with the use of pTG96 (*sur-5::GFP)*[27] as a co-injection marker at 100 ng μl^{-1}. Rescue was scored on the basis of survival on 1 mM levamisole for 16 h.

Tissue-specific rescue

lev-10 complementary DNAs were cloned by PCR after reverse transcription, and sequenced. *SL1* splicing was established by PCR with an SL1 primer and a primer in *lev-10* exon 13, and by sequencing the expressed sequence tag yk796a04.3′. PCR with rapid amplification of cDNA ends (RACE–PCR) was used to localize the polyadenylation site. *lev-10a* and *lev-10b* cDNAs were subcloned into pPD115.62 under the control of the *myo-3* promoter. The CD4 transmembrane domain amplified from the human CD4 cDNA (GenBank accession number M12807) was subcloned in frame into *Pmyo-3::lev-10a* and a stop codon was introduced immediately after the CD4 transmembrane domain. The secreted *gfp-lev-10 s* was obtained by removing the CD4 transmembrane domain from *Pmyo-3::lev-10-CD4* and inserting a GFP cDNA immediately after the *lev-10* signal peptide. All constructs were injected at 20 ng μl^{-1} together with pTG96 (80 ng μl^{-1}) except for *Pmyo-3::gfp-lev-10 s* (10 ng μl^{-1}).

Levamisole dose–response curve

Young adult worms were scored blind for paralysis after 1 h exposure to levamisole. A distance of one body length of forward movement after mechanical stimulus was required to score a worm as non-paralysed.

Electrophysiological studies

Electrophysiological methods were performed as described previously[4]. Muscle recordings were made in the whole-cell voltage-clamp configuration (holding potential −60 mV) with an EPC-10 patch-clamp amplifier and digitized at 1 kHz. Data were acquired by Pulse software (HEKA). The bath solution contained 150 mM NaCl, 5 mM KCl, 5 mM $CaCl_2$, 1 mM $MgCl_2$, 10 mM glucose and 15 mM HEPES, pH 7.35, about 340 mOsm. The pipette solution was prepared as described previously[4]. Subsequent analysis and graphing were performed with Pulsefit (HEKA) and Igor Pro. All statistically derived values are given as means ± s.e.m.

Antibody production and immunocytochemistry

UNC-29: a DNA fragment encoding UNC-29 amino acids 348–431 was inserted into pGEX-3X (Amersham Biosciences). The glutathione-*S*-transferase (GST)–UNC-29

fusion protein was expressed in *Escherichia coli* and purified in accordance with the manufacturer's protocol. Rabbits were injected with 100 μg of fusion protein and boosted three times with 100 μg each.

LEV-10: two synthetic peptides (Eurogentec) corresponding to the LEV-10A amino acids 847–861 and 892–906 were injected into rabbits as described for UNC-29. Both antibodies were purified as described previously[28] by using the fusion proteins GST–UNC-29 or GST–LEV-10A (amino acids 836–906 in pGEX-3X) blotted on nitrocellulose. Immunostaining was performed as described[9]. UNC-29 antibody was used at a dilution of 1:250, and LEV-10 antibody at 1:300. For double-labelling experiments, UNC-17 monoclonal antibody[15] was diluted at 1:500 and incubated for 1 h; after 1 h of washing, UNC-29 or LEV-10 antibodies were incubated overnight. The secondary antibody, Cy3-labelled goat anti-rabbit IgG (H + L) (Jackson ImmunoResearch Laboratories), was diluted at 1:900 and the secondary antibody, Alexa488-labelled goat anti-mouse (Molecular Probes) at 1:200.

Protein extraction and western blotting

A mixed staged population of worms (500 μl) was frozen at −80 °C until use. For extraction, worm pellets were ground under liquid nitrogen and thawed on ice. While thawing, 6–10 volumes of ice-cold homogenization buffer (20 mM HEPES pH 7.4, 10 mM KCl, 1 mM EDTA, 400 μM Pefabloc (Roche) and Complete Mini Protease inhibitor cocktail (Roche)) were added and the suspension was further homogenized with ten strokes with the use of a 2-ml tight-fitting glass tissue homogenizer. Afterwards an equal volume of homogenization buffer containing 0.5 M sucrose was added and the suspension was centrifuged twice at 2,000*g* for 10 min to remove worm debris. The resulting nuclear pellets were pooled and extracted twice with 5 ml of homogenization buffer containing 0.25 M sucrose. The post-nuclear supernatants were pooled and subsequently centrifuged at 150,000*g* for 1 h. Equal amounts (about 30 μg) of the resulting cytosolic supernatant and membrane pellet were separated by SDS–polyacrylamide-gel electrophoresis and blotted onto nitrocellulose membranes. The membranes were subsequently probed with purified anti-LEV-10 serum (dilution 1:1000), anti-UNC-29 (1:600) or anti-VHA-5 (1:3000) (M. Labouesse, unpublished observations) and horseradish-peroxidase-conjugated goat anti-rabbit antibodies (DAKO) and revealed with LumiLight reagents (Roche).

Received 3 June; accepted 30 July 2004; doi:10.1038/nature02893.

1. Lewis, J. A., Wu, C. H., Berg, H. & Levine, J. H. The genetics of levamisole resistance in the nematode *Caenorhabditis elegans*. *Genetics* **95,** 905–928 (1980).
2. Lewis, J. A., Wu, C. H., Levine, J. H. & Berg, H. Levamisole-resistant mutants of the nematode *Caenorhabditis elegans* appear to lack pharmacological acetylcholine receptors. *Neuroscience* **5,** 967–989 (1980).
3. Lewis, J. A. *et al.* Cholinergic receptor mutants of the nematode *Caenorhabditis elegans*. *J. Neurosci.* **7,** 3059–3071 (1987).
4. Richmond, J. E. & Jorgensen, E. M. One GABA and two acetylcholine receptors function at the *C. elegans* neuromuscular junction. *Nature Neurosci.* **2,** 791–797 (1999).
5. Bessereau, J. L. *et al.* Mobilization of a *Drosophila* transposon in the *Caenorhabditis elegans* germ line. *Nature* **413,** 70–74 (2001).
6. Fleming, J. T. *et al. Caenorhabditis elegans* levamisole resistance genes *lev-1*, *unc-29*, and *unc-38* encode functional nicotinic acetylcholine receptor subunits. *J. Neurosci.* **17,** 5843–5857 (1997).
7. Alfonso, A., Grundahl, K., Duerr, J. S., Han, H. P. & Rand, J. B. The *Caenorhabditis elegans unc-17* gene: a putative vesicular acetylcholine transporter. *Science* **261,** 617–619 (1993).
8. Bamber, B. A., Beg, A. A., Twyman, R. E. & Jorgensen, E. M. The *Caenorhabditis elegans unc-49* locus encodes multiple subunits of a heteromultimeric GABA receptor. *J. Neurosci.* **19,** 5348–5359 (1999).
9. Gally, C. & Bessereau, J. L. GABA is dispensable for the formation of junctional GABA receptor clusters in *Caenorhabditis elegans*. *J. Neurosci.* **23,** 2591–2599 (2003).
10. Raizen, D. M., Lee, R. Y. & Avery, L. Interacting genes required for pharyngeal excitation by motor neuron MC in *Caenorhabditis elegans*. *Genetics* **141,** 1365–1382 (1995).
11. McKay, J. P., Raizen, D. M., Gottschalk, A., Schafer, W. R. & Avery, L. *eat-2* and *eat-18* are required for nicotinic neurotransmission in the *C. elegans* pharynx. *Genetics* **166,** 161–169 (2004).
12. Bork, P. & Beckmann, G. The CUB domain. A widespread module in developmentally regulated proteins. *J. Mol. Biol.* **231,** 539–545 (1993).
13. Christensen, E. I. & Birn, H. Megalin and cubilin: multifunctional endocytic receptors. *Nature Rev. Mol. Cell Biol.* **3,** 256–266 (2002).
14. Herz, J. & Bock, H. H. Lipoprotein receptors in the nervous system. *Annu. Rev. Biochem.* **71,** 405–434 (2002).
15. Duerr, J. S., Gaskin, J. & Rand, J. B. Identified neurons in *C. elegans* coexpress vesicular transporters for acetylcholine and monoamines. *Am. J. Physiol. Cell Physiol.* **280,** C1616–C1622 (2001).
16. Okkema, P. G., Harrison, S. W., Plunger, V., Aryana, A. & Fire, A. Sequence requirements for myosin gene expression and regulation in *Caenorhabditis elegans*. *Genetics* **135,** 385–404 (1993).
17. Ono, F., Mandel, G. & Brehm, P. Acetylcholine receptors direct rapsyn clusters to the neuromuscular synapse in zebrafish. *J. Neurosci.* **24,** 5475–5481 (2004).
18. Bredt, D. S. & Nicoll, R. A. AMPA receptor trafficking at excitatory synapses. *Neuron* **40,** 361–379 (2003).
19. Choquet, D. & Triller, A. The role of receptor diffusion in the organization of the postsynaptic membrane. *Nature Rev. Neurosci.* **4,** 251–265 (2003).
20. O'Brien, R. J. *et al.* Synaptic clustering of AMPA receptors by the extracellular immediate-early gene product Narp. *Neuron* **23,** 309–323 (1999).
21. Dalva, M. B. *et al.* EphB receptors interact with NMDA receptors and regulate excitatory synapse formation. *Cell* **103,** 945–956 (2000).
22. Passafaro, M., Nakagawa, T., Sala, C. & Sheng, M. Induction of dendritic spines by an extracellular domain of AMPA receptor subunit GluR2. *Nature* **424,** 677–681 (2003).
23. Tomita, S., Fukata, M., Nicoll, R. A. & Bredt, D. S. Dynamic interaction of stargazin-like TARPs with cycling AMPA receptors at synapses. *Science* **303,** 1508–1511 (2004).
24. Zheng, Y., Mellem, J. E., Brockie, P. J., Madsen, D. M. & Maricq, A. V. SOL-1 is a CUB-domain protein required for GLR-1 glutamate receptor function in *C. elegans*. *Nature* **427,** 451–457 (2004).
25. Stohr, H., Berger, C., Frohlich, S. & Weber, B. H. A novel gene encoding a putative transmembrane protein with two extracellular CUB domains and a low-density lipoprotein class A module: isolation of alternatively spliced isoforms in retina and brain. *Gene* **286,** 223–231 (2002).
26. Michishita, M. *et al.* A novel gene, Btcl1, encoding CUB and LDLa domains is expressed in restricted areas of mouse brain. *Biochem. Biophys. Res. Commun.* **306,** 680–686 (2003).
27. Yochem, J., Gu, T. & Han, M. A new marker for mosaic analysis in *Caenorhabditis elegans* indicates a fusion between hyp6 and hyp7, two major components of the hypodermis. *Genetics* **149,** 1323–1334 (1998).
28. Miller, K. G., Emerson, M. D., McManus, J. R. & Rand, J. B. RIC-8 (Synembryn): a novel conserved protein that is required for $G_q\alpha$ signaling in the *C. elegans* nervous system. *Neuron* **27,** 289–299 (2000).

Supplementary Information accompanies the paper on **www.nature.com/nature**.

Acknowledgements We thank J. Lewis for the *lev-10(x17)* strain, M. Labouesse for the anti-VAH-5 antibodies, J. Rand for the anti-UNC-17 antibodies, M. Han for the pTG96 plasmid, Y. Kohara for the clone yk796a04, A. Fire for the GFP vectors, the *Caenorhabditis* Genetic Center for strains, R. Weimer for critical reading of the manuscript, and I. Nuez and H. Gendrot for technical help. C.G. was supported by a fellowship from the Ministère de la Recherche and by the Association pour la Recherche contre le Cancer. S.E. is an EMBO fellow. This work was funded by the Institut National de la Santé et de la Recherche Médicale and the Association Française contre les Myopathies. J.R. was supported by the NIH grant RO1NS41477-03.

Competing interests statement The authors declare that they have no competing financial interests.

Correspondence and requests for materials should be addressed to J.-L.B. (jlbesse@wotan.ens.fr).
The EMBL database accession numbers for *lev-10a* and *lev-10b* cDNAs are BN000434 and BN000435, respectively.

The rice leaf blast pathogen undergoes developmental processes typical of root-infecting fungi

Ane Sesma & Anne E. Osbourn

The Sainsbury Laboratory, John Innes Center, Colney Lane, Norwich NR4 7UH, UK

Pathogens have evolved different strategies to overcome the various barriers that they encounter during infection of their hosts[1]. The rice blast fungus *Magnaporthe grisea* causes one of the most damaging diseases of cultivated rice and has emerged as a paradigm system for investigation of foliar pathogenicity. This fungus undergoes a series of well-defined developmental steps during leaf infection, including the formation of elaborate penetration structures (appressoria). This process has been studied in great detail[2], and over thirty *M. grisea* genes that condition leaf infection have been identified[3]. Here we show a new facet of the *M. grisea* life cycle: this fungus can undergo a different (and previously uncharacterized) set of programmed developmental events that are typical of root-infecting pathogens. We also show that root colonization can lead to systemic invasion and the development of classical disease symptoms on the aerial parts of the plant. Gene-for-gene type specific disease resistance that is effective against rice blast in leaves also operates in roots. These findings have significant implications for fungal development, epidemiology, plant breeding and disease control.

Because rice is the staple food for half of the global population, rice blast is a constant threat to the world's food supply. Control strategies depend on use of resistant cultivars and application of fungicides, although neither of these methods is particularly effective[4]. The development of durable, environmentally friendly strategies for the control of rice blast disease will depend on a better understanding of the disease process. To this end, the sequence of the *M. grisea* genome has been completed with the objective of gaining an intimate knowledge of the pathogen and of factors governing disease[4]. Recent changes in fungal taxonomy have led to the reclassification of *M. grisea* into the newly established Magnaporthaceae family[5]. This family includes the soil-borne pathogen *Gaeumannomyces graminis*[6,7], which causes the take-all